HHS Public Access

Author manuscript

Sci Transl Med. Author manuscript; available in PMC 2015 March 10.

Published in final edited form as:

Sci Transl Med. 2014 September 24; 6(255): 255ra132. doi:10.1126/scitranslmed.3008810.

Treatment of heterotopic ossification through remote ATP hydrolysis

Jonathan R. Peterson[1], **Sara De La Rosa**[1], **Oluwatobi Eboda**[1], **Katherine E. Cilwa**[2], **Shailesh Agarwal**[1], **Steven R. Buchman**[1], **Paul S. Cederna**[1,3], **Chuanwu Xi**[4], **Michael D. Morris**[5], **David N. Herndon**[6], **Wenzhong Xiao**[7], **Ronald G. Tompkins**[7], **Paul H. Krebsbach**[8], **Stewart C. Wang**[1], and **Benjamin Levi**[1,*]

[1]Department of Surgery, University of Michigan Medical School, Ann Arbor, MI 48109, USA

[2]Department of Regenerative Medicine, Naval Medical Research Center, Silver Spring, MD 20910, USA

[3]Section of Plastic Surgery, Department of Biomedical Engineering, University of Michigan Health System, Ann Arbor, MI 48109, USA

[4]Department of Environmental Health Sciences, University of Michigan School of Public Health, Ann Arbor, MI 48109, USA

[5]Department of Chemistry, University of Michigan, Ann Arbor, MI 48109, USA

[6]Department of Surgery, University of Texas Medical Branch at Galveston, and Shriners Hospitals for Children, Galveston, TX 77550, USA

[7]Department of Surgery, Massachusetts General Hospital, Boston, MA 02114, USA

[8]Department of Biologic and Material Sciences, University of Michigan School of Dentistry, Ann Arbor, MI 48109, USA

Abstract

Heterotopic ossification (HO) is the pathologic development of ectopic bone in soft tissues because of a local or systemic inflammatory insult, such as burn injury or trauma. In HO, mesenchymal stem cells (MSCs) are inappropriately activated to undergo osteogenic differentiation. Through the correlation of in vitro assays and in vivo studies (dorsal scald burn

*Corresponding author. blevi@med.umich.edu.

Author contributions: B.L., S.C.W., P.H.K., R.G.T., D.N.H., M.D.M., P.S.C., S.R.B., and J.R.P. designed the research. J.R.P., S.D.L.R., S.A., and C.X. performed in vitro experiments. J.R.P., S.D.L.R., O.E., K.E.C., and S.A. performed in vivo experiments. D.N.H., W.X., R.G.T., and B.L. performed microarray analysis. J.R.P., S.D.L.R., O.E., K.E.C., and B.L. analyzed the data. J.R.P., S.A., and B.L. interpreted the data and performed statistical analysis. J.R.P. and B.L. wrote the manuscript. S.C.W., P.H.K., R.G.T., D.N.H., M.D.M., and P.S.C. provided supervisory support.

SUPPLEMENTARY MATERIALS

www.sciencetranslationalmedicine.org/cgi/content/full/6/255/255ra132/DC1

Competing interests: A patent application for part of this work has been filed by the University of Michigan (application no. 61707228).

Data and materials availability: Human gene expression data from fat are available in the Inflammation and Host Response to Injury Large Scale Collaborative Research Program TRDB (http://www.gluegrant.org/). The Gene Expression Omnibus series accession number for the microarray data is GSE37069.

with Achilles tenotomy), we have shown that burn injury enhances the osteogenic potential of MSCs and causes ectopic endochondral heterotopic bone formation and functional contractures through bone morphogenetic protein–mediated canonical SMAD signaling. We further demonstrated a prevention strategy for HO through adenosine triphosphate (ATP) hydrolysis at the burn site using apyrase. Burn site apyrase treatment decreased ATP, increased adenosine 3′,5′-monophosphate, and decreased phosphorylation of SMAD1/5/8 in MSCs in vitro. This ATP hydrolysis also decreased HO formation and mitigated functional impairment in vivo. Similarly, selective inhibition of SMAD1/5/8 phosphorylation with LDN-193189 decreased HO formation and increased range of motion at the injury site in our burn model in vivo. Our results suggest that burn injury–exacerbated HO formation can be treated through therapeutics that target burn site ATP hydrolysis and modulation of SMAD1/5/8 phosphorylation.

INTRODUCTION

Heterotopic ossification (HO) is a complex, reactive, musculoskeletal condition characterized by bone formation in soft tissues and joint spaces, which frequently complicates trauma, burns, and orthopedic surgeries. A large number of major burn patients and more than 50% of soldiers sustaining blast injuries develop HO in at least one of their joints, often distant from the site of burn or trauma, making it difficult to target one specific region or cell population (*1*, *2*). No current treatment or prophylactic measures are taken to prevent this clinically devastating complication.

Current treatment approaches to HO include bisphosphonates, which can cause osteonecrosis, glucocorticoids and external beam radiation, which impair wound healing, and nonsteroidal anti-inflammatory drugs, which impair fracture healing and have negative cardiovascular effects. Despite these treatments and surgical excision, 75% of patients have limited range of motion (ROM) postoperatively (*3*, *4*).

Current therapeutics fail to target the key signaling pathway involved in trauma/burn-induced HO: canonical SMAD-mediated bone morphogenetic protein (BMP) signaling. Thus, either topical treatments directed at the site of burn injury or systemic treatments that target canonical SMAD-mediated BMP signaling would likely improve current treatment strategies.

BMP ligands facilitate the assembly of BMP type I and type II receptors to activate downstream SMAD effector proteins 1, 5, and 8 (SMAD1/5/8), otherwise known as “canonical” BMP-SMAD signaling. After their phosphorylation by type II receptors, such as BMPRII and ACTRIIA, activated BMP type I receptors, such as ALK2, ALK3, and ALK6, can then phosphorylate SMAD proteins. ALK2 mutations have been well described to play a role in patients with fibrodysplasia ossificans progressiva (FOP), where patients develop progressive HO (*5*–*7*). Recent studies have implicated ALK2 as playing a more central role in cartilage condensation and ALK3 as playing a more central role in osteogenic differentiation (*8*). Thus, it seems logical to target ALK2 and ALK3 to inhibit both early cartilage deposition and subsequent endochondral bone formation.

Trauma/burn-induced HO forms through an endochondral ossification process, which begins with the congregation of mesenchymal stem cells (MSCs), followed by their differentiation into chondrocytes (*9*). To understand likely key pathways involved in human tissue, we surveyed a repository of tissue from 244 burn patients, looking at a subset of genes related to BMP-mediated canonical SMAD signaling that is known to play a role in congenital HO. The expression of these genes was assessed by interrogation of genomic data generated to determine the burn-induced changes in adipose tissue after severe burn injury. We analyzed the genomic data from burn patients as well as the in vitro osteogenic capacity of the MSCs from burn patients to understand the "osteogenic environment" and effect on BMP-SMAD signaling created by a burn injury.

Most studies investigating HO describe recombinant BMP protein, cell implantation, or the use of mutant mice (*10*). Although valid, these models do not represent the HO that is formed de novo in burn and trauma patients. Thus, we used a tenotomy and remote burn injury model to establish the mechanism, osteogenic course, and treatments for burn-induced HO. We demonstrate that after Achilles tenotomy and concomitant remote burn injury, HO results from early inflammation and hypervascularization followed by endochondral ossification. Furthermore, we demonstrate that the osteogenic potential and differentiation capacity of MSCs from mice and humans are enhanced after remote cutaneous burn. Additionally, in the present study, we mitigate BMP signaling and burn-induced HO by directly targeting the canonical SMAD pathway with small-molecule inhibition.

Given the role of inflammation and the benefits of a topical burn treatment, we also targeted adenosine triphosphate (ATP) at the burn site distant from the site of HO formation. We demonstrate that through ATP hydrolysis at the site of burn injury, we can inhibit BMP signaling and bone formation at the site of HO. Apyrase is an enzyme that hydrolyzes both ATP and ADP (adenosine diphosphate) to AMP (adenosine monophosphate), causing an increase in intracellular adenylate cyclase activity and cyclic AMP (cAMP), which inhibits SMAD1/5/8 phosphorylation (*11*). We demonstrate the inhibitory effect of apyrase on HO formation and joint contractures through cAMP inhibition of SMAD1/5/8 phosphorylation.

RESULTS

Burn injury stimulates BMP-mediated canonical SMAD signaling and osteogenic differentiation of human MSCs

MSCs, which are present throughout adipose, muscle, and mesodermal tissues, are the primary cells responsible for HO. During burn debridements, the adipose tissue and adipose-derived MSCs are easily accessible and present in large quantities. We analyzed adipose tissue from 244 burn patients within 96 hours of their burn injury. Tissue samples were collected from patients who had burns over at least 20% of the total body surface area (TBSA) and required at least one excision and grafting procedure. Gene expression of these patients was compared to that of 35 control patients. There was a clear correlation and up-regulation of the canonical SMAD signaling pathway in addition to downstream up-regulation of runt-related transcription factor-2 (*RUNX2*), the primary osteogenic gene transcription regulator (Fig. 1 and table S1). Additionally, we observed a direct link between SMAD1/5/8 signaling and adenosine receptors, because direct stimulation of CREBBP

activates the adenosine A2a receptor. These findings led us to hypothesize that the BMP pathway and ATP signaling both played a role in burn/trauma-induced HO.

To verify these array findings, we first compared MSCs from adipose tissue of burn patients within the first 3 days of their burn injury with those from sex- and age-matched control patients. Osteogenic-related transcription factors *RUNX2* and osteocalcin (*OCN*) were markedly increased after burn injury (Fig. 2A). Furthermore, burn injury increased early human MSC (hMSC) osteogenic differentiation, as demonstrated by alkaline phosphatase (ALP) staining of cells and a greater than 10-fold increase in ALP enzyme activity after treatment with osteogenic differentiation medium (ODM) to quantify osteogenic induction (Fig. 2, B and C). Similarly, hMSCs harvested from burn patients deposited significantly more mineralized extracellular matrix (detected by alizarin red stain) after ODM treatment ($P = 0.002$; Fig. 2, B and D). Analysis of BMP-mediated canonical SMAD pathway with ODM treatment showed an increase in BMP-2 expression (Fig. 2A) and activated pSMAD1/5/8 in burn hMSCs, indicating an increase in BMP signaling (Fig. 2,E and F). Thus, burn injury increases the osteogenic capacity of hMSCs, which can be partially explained by an increase in canonical SMAD-dependent BMP signaling.

Burn injury increases osteogenic differentiation and BMP signaling in a mouse burn model

We performed a dorsal scald burn covering 30% surface area of the mouse and harvested inguinal MSCs 2 hours after burn injury. MSCs harvested from the inguinal fat pads of mice (mMSCs) with dorsal burn injuries showed enhanced osteogenic capacity compared to non-burn controls (Fig. 3A). ODM-treated mMSCs from mice with burn injuries also demonstrated an increase in early osteogenesis by ALP stain and quantification (Fig. 3, B and C). End matrix mineralization, detected by alizarin red, was also increased in mice with burn injury compared to non-burn control (Fig. 3, B and D). BMPR1 signaling in mMSCs was increased after burn injury, as demonstrated by an increase in phosphorylation of SMAD1/5/8 by Western blot analysis (Fig. 3, E and F). The use of a dorsal burn and Achilles tenotomy model allowed for the evaluation of mesenchymal cell osteogenicity distant from the site of inflammation. Clinically, these findings correlate with the fact that burn patients can develop HO at sites remote from their burn injury and almost always develop HO in a joint that has not sustained direct trauma.

Small-molecule inhibition of BMP signaling inhibits osteogenic differentiation of mMSCs after burn injury

Having demonstrated the key role of BMP signaling in burn-induced MSC osteogenic differentiation, we next set out to target this pathway through small-molecule BMP inhibition. Supplementation of ODM with LDN-193189, a BMPR1 inhibitor, caused a substantial decrease in mMSC osteogenic differentiation and mineralization (Fig. 3, G and H). Thus, similar to congenital forms of HO, BMP signaling is essential to mMSC osteogenic differentiation (*7*).

ATP hydrolysis mitigates burn-induced BMP signaling and osteogenic differentiation in mMSCs

Although LDN-193189 inhibition of MSC osteogenic differentiation is effective, such small molecules have a side effect profile that currently precludes them from clinical translation (*12*). Thus, we next set out to explore a strategy that targeted burn site inflammation using a compound to cleave the phosphate off ATP, and thereby deactivate it. To assess the effect of burn injury and ATP hydrolysis on MSC osteogenic differentiation, mMSCs were harvested from C57BL/6 mice after burn injury alone or burn injury plus topical application of an ATP hydrolyzing agent (apyrase) to the burn site. mMSCs harvested from apyrase-treated mice after burn injury demonstrated less expression of *Runx2* and *Ocn* and less ALP staining and enzyme activity after ODM treatment (Fig. 3, A to C). This difference in gene expression corresponded with a decrease in bone matrix mineralization (Fig. 3, B and D). Additionally, phosphorylation of SMAD1/5/8 in mMSCs was abrogated by apyrase treatment (Fig. 3, E and F). To more fully stimulate the BMP pathway, we added recombinant BMP-2 ligand to ODM and found that apyrase treatment still decreased mMSC osteogenic differentiation (Fig. 4, A and B). These findings imply that burn site ATP hydrolysis decreases BMP signaling and osteogenic differentiation of mMSCs.

Burn-mediated MSC osteogenesis is related to adenosine signaling

Recent studies demonstrated the presence and activities of adenosine and purinogenic receptors during bone formation (*13, 14*). We demonstrated significantly increased extracellular ATP in mMSCs 2 hours after burn injury ($P = 0.038$). The elevated ATP was reduced with topical application of apyrase at the burn site (Fig. 4C). Concurrently, intracellular cAMP was reduced in mMSCs from mice with burn injuries when compared to mMSCs from non-burn or apyrase-treated mice (Fig. 4D). Increasing cAMP reduces osteogenic differentiation through inhibition of SMAD1/5/8 phosphorylation (*11*). Our array of adipose tissue from burn patients implicated downstream enhancement of RUNX2 and type I collagen expression through adenosine 2A and 2B receptors (Fig. 1). Thus, we next interrogated adenosine receptors in our mouse model with and without burn injury and apyrase treatment. On the basis of qRT-PCR assays for adenosine receptors, we noted an increase in product after ATP cleavage by apyrase (Fig. 4E). By limiting extracellular ATP and increasing intracellular cAMP, apyrase limits the pro-osteogenic response to burn injury and mitigates future HO development through inhibition of SMAD1/5/8 phosphorylation (Fig. 4F).

HO formation from a burn injury and Achilles tenotomy occurs through endochondral ossification and generates a bone marrow niche

In addition to a dorsal burn injury, we also introduced an Achilles tenotomy to analyze the effect of burn injury on tenotomy-induced HO. Notably, inflammation has proven to be an important precursor to HO formation in patients with FOP (*15*). Similarly, in our model, a robust inflammatory response was seen by semiquantitative assessment of the size of the ankle region 1 and 3 weeks after surgery and by enzyme-linked immunosorbent assay (ELISA) measuring serum tumor necrosis factor–α (TNFα) hours after injury (fig. S1). Inflammation was followed by chondrogenesis, as demonstrated by SOX9 and collagen-2

signaling (Fig. 5A). Additionally, the morphology of the heterotopic bone in a pentachrome stain demonstrated cartilage at 3 weeks, followed by mature osteoid at 9 weeks (Fig. 5, A and B). In addition to the endochondral bone formation, we also observed early angiogenic signaling by CD31 staining at 5 days and the appearance of mature bone marrow stroma within mature cortical bone at 9 weeks (Fig. 5, B and C). Vascularity is also known to drive MSC chondrogenesis and osteogenic differentiation preceding reactive bone formation (*16*).

Global SMAD1/5/8 inhibition prevents HO

To verify the key role of BMP signaling through the canonical SMAD pathway for in vivo HO formation in our model, we injected LDN-193189 into mice immediately after their tenotomy and burn injury and every day thereafter. We found that this global SMAD blockade decreased formation of bone at the tenotomy site (Fig. 5, D and E). Additionally, LDN-193189 injection caused a greater percentage decrease in HO formation in those mice with a burn injury and tenotomy compared to a tenotomy alone (Fig. 5, D and E). This small molecule did not cause osteopenia of the contralateral uninjured limb (fig. S2). The inhibition of HO by LDN-193189 demonstrates that SMAD1/5/8 plays a key signaling role in trauma/burn-induced HO, which is similar to key signaling pathways present in FOP models (*5*, *7*).

Apyrase treatment abrogates osteogenic and BMP signaling at sites remote from burn injury

To assess in vivo HO formation and its functional consequences, mouse Achilles tenotomy sites were analyzed with and without a remote burn injury and with and without topical apyrase treatment at the burn site. Osteogenic proteins RUNX2 and OCN were increased at the tenotomy site in the burn group compared to non-burn and apyrase-treated groups, as determined by immunohistochemistry (Fig. 6A). Consistent with osteogenic up-regulation, BMP signaling resulting in phosphorylation of pSMAD1/5/8 was also increased after burn injury and inhibited by apyrase treatment of the burn site (Fig. 6A). These results demonstrate that burn injury increases endochondral bone formation, which is inhibited by apyrase treatment of the burn site.

Apyrase treatment of the burn injury inhibits tenotomy site HO and improves ROM

Next, HO volume was assessed with biweekly μCT scans of the tenotomized leg as well as the contralateral uninjured leg. Application of apyrase to the burn site reduced HO formation detected by μCT at the tenotomy site when compared to the untreated burn, as early as 3 weeks after injury (Fig. 6, B and C). We found a marked decrease in bone formation at 7 to 9 weeks in mice treated with apyrase. Decreased bone formation correlated with ROM at the ankle when a constant force was applied (Fig. 6, D and E). The HO formation occurred remotely from surrounding muscle and periosteum, indicating a different pathogenesis than that of FOP, in which HO normally forms in muscle. Consistent with our μCT findings, histomorphometry showed that mice with burn injury had the thickest cortical bone, and apyrase treatment decreased the amount of heterotopic osteoid (Fig. 6, F and G).

Thus, apyrase treatment of the burn site inhibited distant joint HO and improved functional ROM. Apyrase treatment did not cause osteopenia (fig. S3). Because the topical use of

apyrase would be limited to patients who sustain burn injuries, we also assessed the efficacy of apyrase applied at the tenotomy site and found that local application also limited HO formation (Fig. 6, B and C). Furthermore, after identifying ectopic bone reduction with apyrase or LDN-193189 treatment in this model, we tested combination therapy with topical apyrase application followed by daily LDN-193189 injections and saw a reduction similar to the use of LDN-193189 alone (fig. S4). Finally, to test the effect of long-term, global anti-inflammatory treatment in our model, celecoxib was injected daily into mice after tenotomy and burn, and showed reduced HO formation compared to mice injected with vehicle control (fig. S5).

Raman spectroscopy detects differences in apyrase-treated mice

To elucidate the chemical composition of HO, the tenotomy sites were evaluated by high-resolution Raman spectroscopy (*10, 17*). In soft tissue areas, the primary band near the 958 cm^{-1} bone mineral peak occurred at a higher wave number and lower intensity when normalized to the 1001 cm^{-1} phenylalanine peak, indicating that little to no mineral was present (Fig. 6, H and I). Decreased mineral intensity and differences in MTMR and crystallinity (width of bone mineral band) for similar regions of HO development were observed in mice receiving apyrase to the burn site (Fig. 6, H to K).

DISCUSSION

In addition to burn and trauma patients, who are at risk for HO, more than 1 million patients per year receive joint replacements in the United States, and 20% of these patients will develop HO. After joint revision surgeries, more than 80% of patients develop HO, making these an enormous medical and financial burden. In addition, more than 20% of spine surgery and traumatic brain injury patients develop HO, and HO has even been reported to form outside the skeleton in regions of chronic inflammation, including the abdominal wall and amputation sites (*18, 19*). Despite the large incidence of HO in commonly performed operations, we currently lack an understanding of the key pathways that cause burn/trauma-induced HO and treatment strategies that could prevent it.

Here, we noted an up-regulation in the expression of genes associated with canonical SMAD signaling and osteogenic gene transcription in adipose tissue from burn patients. We then analyzed the hMSCs from a second set of burn patients. The gene expression profile of the hMSCs correlated with the increased canonical SMAD signaling and osteogenic capacity in the adipose tissue of the first set of burn patients.

Similarly, in our burn mouse model, enhanced BMP signaling through the canonical SMAD pathway in mMSCs and at the tenotomy site had a marked effect on osteogenic signaling and HO formation. Heterotopic lesions developed from an endochondral ossification process and were larger in mice with a concomitant burn injury. In congenital forms of HO, such as FOP, a similar up-regulation of BMP-mediated SMAD signaling stimulates endochondral HO formation (*7*). Additionally, recent studies analyzing the role of nerve injury and HO formation implicate BMP as a central signaling pathway (*20*). We saw that global anti-inflammatory treatment with celecoxib reduced HO formation in our model. Furthermore, targeting ATP hydrolysis at the burn wound site through apyrase or systemic inhibition of

canonical SMAD signaling through LDN-193189 injection decreased the osteogenic capacity of mMSCs and tenotomy site HO formation, and improved ankle ROM. This demonstrates that a small-molecule BMP inhibitor, LDN-193189, with relatively broad activity against ALK2 and ALK3 affects bone formation in the trauma/burn injury model of HO.

Although topical apyrase may have limited use outside of burn injury, LDN-193189 can be injected systemically or locally, and celecoxib can be taken orally and thus may offer a potential treatment for other forms of HO, such as those that develop after joint arthroplasty, nerve or spinal cord injury, or local trauma. Furthermore, direct apyrase injection might be an option. Even more promising is the fact that these compounds do not appear to cause global osteopenia or to have a negative effect on already differentiated osteoblasts.

Most animal models of HO require a genetic mutation, the implantation of pluripotent cells, or muscle trauma for bone to form (*7*). In our model, HO was completely remote from the local muscles (gastrocnemius and soleus) and periosteum. Further analysis of the pathway in other trauma-induced forms of HO, including those described by Tannous *et al.* (*21*, *22*), might improve treatment of wounded soldiers.

Our results confirm a link between burn injury and BMP signaling in MSCs, which is particularly important for trauma patients (*23*). Additionally, we show strong evidence that inflammation caused by a burn injury increases osteogenic signaling specifically through SMAD1/5/8 signaling in MSCs. Mice that had burn injury with Achilles tenotomy and received LDN-193189 injection did not develop HO, suggesting that BMP signaling plays an important role in osteogenesis induced by inflammation.

Furthermore, we demonstrated that application of apyrase to the burn site decreases mMSC osteogenic differentiation, BMP signaling, and in vivo HO formation. Our results suggest that apyrase limits the pro-osteogenic response to burn injury by decreasing extracellular ATP and increasing intracellular cAMP. Increases in cAMP have been shown to inhibit osteogenic differentiation by inhibiting SMAD1/5/8 phosphorylation, a process that may occur with apyrase application as well (*24*). Also of note, several well-executed studies have used phosphodiesterase inhibitors, such as IBMX, which are capable of increasing intracellular cAMP to stimulate adipogenic differentiation of MSCs (*25*, *26*). Such small molecules should be further investigated as potential treatment options for HO. Notably, apyrase applied to the burn site exerts its influence at the remote burn site, and mMSCs collected from the unburned inguinal fat pads are susceptible to its influence. Therefore, we may be able to avoid the toxicity associated with systemic drugs that have been previously trialed to decrease inflammation and prevent HO (*27*). The finding that inhibition of BMP signaling or ATP breakdown can each independently abrogate in vitro and in vivo bone production provides further evidence that ATP and BMP are both involved in bone development. Notably, we have previously demonstrated that apyrase treatment also improves burn wound healing, making it an attractive candidate for burn treatment and HO prevention (*28*). Finally, the central role of inflammation was confirmed by our findings that the use of celecoxib, a cyclooxygenase-2 inhibitor, markedly decreased HO formation at the

tenotomy site. Current clinical trials are ongoing to use celecoxib in burn and orthopedic patients at high risk of forming HO.

Important limitations exist in our study. First, our large human genomic analysis analyzes adipose tissues. Having a similar array of heterotopic bone tissues from burn patients would allow for further understanding of the role of burn injury on HO formation. Second, in our mouse in vitro model, we have chosen to analyze MSCs from adipose tissue. We prefer the adipose tissue because it allows the study of MSCs at a remote site from the direct injury, lets us compare the results to our human data, and harbors MSCs capable of multilineage differentiation, including bone.

In conclusion, our burn tenotomy model provides a system to examine the role of burn injury on HO formation and for testing therapeutics that target global or local inflammation. Burn injury increases the osteogenic potential of MSCs and HO formation at a tenotomy site through canonical SMAD-dependent BMP signaling. Additionally, apyrase treatment of the burn site decreases MSC osteogenic differentiation and SMAD1/5/8-dependent BMP signaling, and, most importantly, abrogates HO formation and joint contractures. Similarly, LDN-193189, a small-molecule inhibitor of canonical SMAD signaling, diminishes MSC osteogenesis and HO formation. These findings identify a possible mechanism by which HO forms after a major inflammatory injury such as a burn. Finally, these results also point to possible therapeutic approaches to prevent and treat HO in burn patients by targeting burn site ATP levels or global canonical SMAD signaling.

MATERIALS AND METHODS

Study design

The objective of this research was to analyze the effect of burn injury on MSC osteogenesis and HO. Additionally, we set out to assess the effect of ATP hydrolysis at the burn site and global SMAD1/5/8 signaling inhibition on MSC osteogenic differentiation and HO. Hypotheses that came after the initiation of the study included the endochondral nature of the HO formed. The research subjects included a large cohort of 244 burn and 35 control patients for microarray analysis. hMSCs were harvested from female burn patients within the first 3 days of their burn injury ($n = 3$) and from age-matched control patients ($n = 3$). C57BL/6 mice were used for in vivo experiments and as a source of mMSCs. Our mouse sample size was selected on the basis of a power analysis and previous studies of similar design (*17*). There was no change in the number of animals over the course of the study, and six animals were used in each group for in vivo studies ($n = 6$). For cell culture, MSCs were harvested from three mice per group, which was determined to be the required number to establish a successful primary culture. These cells were passaged three times to ensure a homogeneous distribution. Endpoints were all based on previous studies of MSCs. Osteogenic differentiation endpoints were 3 and 7 days for hMSCs and 7 and 14 days for mMSCs. Day 0 undifferentiated cells were also used as a control. The endpoints for in vivo experiments were selected when there were no longer significant changes noted in HO development, as determined by longitudinal μCT scans. The data reported here represent one iteration of the in vivo Achilles tenotomy model; in vitro experiments were run in triplicate. This study is a controlled laboratory experiment, and unbiased measurements were ensured

by blinding of two independent observers in procedures where visual quantification was required (ROM measurement, inflammation at tenotomy site). All data were included, and no outliers were excluded from the study.

Ethics statement

All procedures involving humans were approved by the Institutional Review Boards of the University of Michigan (HUM0005190), the University of Texas Medical Branch, the University of Florida, and Massachusetts General Hospital. All procedures involving animals were approved by the Institutional Animal Care and Use Committee of the University of Michigan (PRO0001553).

Chemicals, supplies, and animals

Dulbecco's modified Eagle's medium (DMEM), fetal bovine serum (FBS), and penicillin/streptomycin were purchased from Gibco Life Technologies. BMP-2 was purchased from R&D Systems. All other chemicals, unless otherwise specified, were obtained from Sigma-Aldrich. C57BL/6 mice were purchased from Charles River.

Patient enrollment and sampling for ingenuity array

Two hundred forty-four burn patients (0 to 83 years) were enrolled between 2000 and 2009 at one of four burn centers if admission occurred within 96 hours after injury, at least 20% of the TBSA was affected, and at least one excision and grafting procedure was required. Thereafter, study participants were treated according to uniform standard operating procedures implemented at all participating centers. Additionally, 35 healthy control subjects (16 to 55 years) were recruited between 2004 and 2007. The genes that we examined were identified as significant with a false discovery rate (FDR) <0.001 and fold change ≥1.5.

Analysis of time course gene expression data

Waste adipose specimens were obtained from patients with severe burns. Infants (<1 year old) were not included in this study. Specimens were immediately stabilized using RNAlater (Ambion), and total cellular RNA was extracted using a commercial RNA purification kit (RNeasy, Qiagen). Biotinylated complementary RNA was generated from 1 μg of total cellular RNA using the 3′ IVT Express Kit and protocol from Affymetrix, and hybridized onto an HU133 Plus 2.0 GeneChip (Affymetrix). Details of the protocols used for stabilizing the tissue specimens and sample processing for gene expression analysis have been previously published (*29*).

EDGE (Extraction of Differential Gene Expression) was used to estimate the significance of expression changes for each gene by 1000 random permutations. Significant genes were selected by FDR <0.001 and fold change ≥1.5.

Cell harvest and in vitro culture assays

hMSCs were harvested from female burn patients without major comorbidities within the first 3 days of their thermal burn injury, which covered at least 20% TBSA (30 to 61 years, *n*

= 3). As controls, lipoaspirates derived from three age-matched female patients, with mean body mass index of 27.3 kg/m^2 and lacking any major medical comorbidities, were used as previously described (21 to 53 years, n = 3) (30). Mouse MSCs were harvested from the inguinal fat pads at 2 hours after burn injury or burn + apyrase application [200 μl of 400 U/ml in phosphate-buffered saline (PBS)]. Non-burn control MSCs (n = 3 per group) were used as previously described (*30*). Cells were grown in standard growth medium (DMEM, 10% FBS, 1% penicillin/streptomycin) and passaged three times by trypsinization before being used for osteogenic assays. Osteogenic assays were performed in triplicate with exposure to ODM [DMEM, 10% FBS, 10 mM β-glycerophosphate, ascorbic acid (100 μg/ml), 1% penicillin/streptomycin]. Early osteogenic differentiation was assessed by ALP stain after 3 days in ODM for hMSCs and after7 days for mMSCs, as previously described (*31*). Quantification of ALP protein concentration was also completed at the same time points using Pierce BCA protein assay (Thermo Fisher). Alizarin red staining for bone mineral deposition and photometric quantification were completed at 1 week for hMSCs and at 2 weeks for mMSCs as previously described (*31*). For select experiments, BMP-2 (200 ng/ml), apyrase (4 U/ml), LDN-193189 (250 nM), or vehicle control (dimethyl sulfoxide for LDN-193189, PBS for all others) was added to ODM.

Quantification of cAMP and ATP signaling in mMSCs

To quantify extracellular ATP and intracellular cAMP in mMSCs, bioluminescent (BioAssay) or colorimetric (Cell Biolabs) kits were used, respectively, according to the manufacturers' specifications.

Polymerase chain reaction

RNA was harvested from cells after 7 days of exposure to ODM with RNeasy Mini Kit (Qiagen). RNA (1 μg) was reverse-transcribed to complementary DNA using TaqMan Reverse Transcription Reagents (Applied Biosystems). qRT-PCR was completed using SYBR Green PCR Master Mix (Applied Biosystems) as previously described (*32*, *33*). Specific primers for these genes corresponded to their PrimerBank sequences and can be found in table S2.

Western blot analysis

After 7 days of exposure to ODM, mMSCs and hMSCs were collected and assayed with standard immunoblotting technique as previously described (32). Primary antibodies were chosen as follows: anti–phospho-SMAD1/5/8, anti-SMAD5, and anti–α-tubulin (Cell Signaling), and applied in a 1:1000 dilution. Secondary, horseradish peroxidase–conjugated antibody was applied at 1:2000 dilution (Cell Signaling). Enhanced chemiluminescence substrate (SuperSignal West Pico, Thermo Scientific) was used for visualization, and densitometry analysis was completed with bands normalized to the loading controls (α-tubulin).

Burn injury and Achilles tenotomy models

Partial-thickness scald injury was performed as previously described (*17*). In brief, mice received a 30% TBSA partial thickness burn injury with exposure to 60°C water for 18 s.

Apyrase treatment groups received topical application of 200 μl of apyrase (400 mU/ml) in PBS immediately after burn injury. In our in vivo model, all mice received an Achilles tenotomy on the left leg after burn, burn + apyrase, or non-burn injury (n = 6 per group) as previously described (*17*). A second cohort also received Achilles tenotomy with or without concurrent burn injury and then received daily intraperitoneal injection of LDN-193189 [6 mg/kg of suspension (1.5 mg/ml) in normal saline] or vehicle control (n = 6 per group). A third cohort received Achilles tenotomy, burn injury, and one of the following treatments: topical apyrase + daily LDN-193189 injection, local application of apyrase at the tenotomy site before incision closure, or daily intraperitoneal injection of celecoxib (30 mg/kg) (n = 3 per group).

Histologic processing and analyses

At 5 days (n = 3 per group) and 9 weeks (n = 6 per group) postoperatively, animals were euthanized and histology was performed as previously described (*17*). Decalcification of whole lower limbs was completed with 19% EDTA solution for 28 to 42 days or until there was radiographic evidence of decalcification by x-ray at 4°C, and then paraffin-embedded. Sagittal or transverse sections with a width of 5 mm were mounted on Superfrost Plus slides (Fisher Scientific). Aniline blue, H&E, and pentachrome staining were performed for histologic and histomorphometric analysis (*33*).

Immunohistochemistry of osteogenic proteins and SMAD pathway

Rehydrated slides were blocked with 10% goat serum; the primary antibodies used included rabbit polyclonal anti-pSMAD1/5/8, anti-OCN, anti-RUNX2, anti-SOX9, and anti–collagen-2 in 1% rabbit serum (1:80 dilution, Santa Cruz Biotechnology). The appropriate biotinylated secondary antibodies were used in 1:1000 dilution (Vector Laboratories). Visualization was performed with diaminobenzidine (Zymed Laboratories), as previously described (*33*).

Analysis of ankle ROM

Nine weeks after tenotomy, mice were briefly anesthetized and assessed for ROM at the tenotomy site by extending the ankle with a 75-g weight attached to the hindpaw to ensure full, uniform extension. Photographs were taken with the extended ankle centered on a disk of standardized size and distance. The angle of maximum extension was then assessed by two independent, blinded observers using the ruler tool in Adobe Photoshop.

μCT imaging

μCT scan (Siemens Inveon) images were obtained with the following settings: 80 kV, 500 μA, and 1300-ms exposure. Three hundred sixty projections of 48-mm voxel size were taken after calibration with known density standards. The region of interest (ROI) corresponding to the location of HO formation was segmented on the basis of anatomical landmarks, Hounsfield units, and observer identification to define and subtract the volume of original cortical bone structures from the ROI. The remaining bone mineral in the soft tissues was quantified for HO bone volume using standard protocols (*17*).

Raman spectroscopy

Spectroscopic measurements were taken 9 weeks after tenotomy using a previously described microprobe system (*10*). Briefly, cross-sections at the tenotomy site were made with a diamond-tipped exact bandsaw without any fixation or embedding. Spectra of these fresh tissue samples were taken on an ex vivo Raman microscopy platform over 100-mm areas selected according to μCT scans for areas containing or not containing ectopic bone.

Spectra were preprocessed for removal of cosmic spikes, grating-induced anamorphic magnification (curvature), and correction of spectrograph/ detector alignment. Low-order polynomial fitting was used to correct for fluorescence background. Mineral content was defined as corresponding to the height of the intense PO_4^{-3} ν_1 stretch (958 cm^{-1}), and crystallinity was measured as the width of this band. The height of the amideI band (1660 cm^{-1}) was used as the measure of matrix content.

Statistical analysis

Mean values are represented as bars in graphs; error bars signify 1 SD. A two-sided *t* test or one-way ANOVA was used to compare means and determine significance, which was defined as $P < 0.05$. Levene's test was used to exclude inequality of SDs. Post hoc analysis to compare more than two groups included Tukey's honestly significant difference test or Games-Howell analysis if Levene's test indicated inequality of variance. The original data for all figures are in table S3.

Supplementary Material

Refer to Web version on PubMed Central for supplementary material.

Acknowledgments

We thank A. Fair and the Center for Molecular Imaging at the University of Michigan for assistance with μCT imaging and analysis, and E. Salzman for assistance with molecular biology.

Funding: B.L. was funded by 1K08GM109105-01 and Plastic Surgery Foundation National Endowment Award. This research was partially supported by NIH grant R01GM098350-02 to C.X. and S.C.W.; NIH grant R01 AR055222 to M.D.M.; National Institute on Disability and Rehabilitation Research (grants H133A070026 and H133A70019), NIH (grants P50-GM60338, R01-GM56687, and T32-GM8256), and Shriners Hospitals for Children (grants 85500 and 71008) to D.N.H.; and NIH grant U54-GM062119 to R.G.T. and its legacy grant R24-GM102656 to W.X. for the Trauma-Related Database (TRDB).

REFERENCES AND NOTES

1. Forsberg JA, Potter BK. Heterotopic ossification in wartime wounds. J. Surg. Orthop. Adv. 2010; 19:54–61. [PubMed: 20371008]
2. Potter BK, Forsberg JA, Davis TA, Evans KN, Hawksworth JS, Tadaki D, Brown TS, Crane NJ, Burns TC, O'Brien FP, Elster EA. Heterotopic ossification following combat-related trauma. J. Bone Joint Surg. Am. 2010; 92(Suppl. 2):74–89. [PubMed: 21123594]
3. Hunt JL, Arnoldo BD, Kowalske K, Helm P, Purdue GF. Heterotopic ossification revisited: A 21-year surgical experience. J. Burn Care Res. 2006; 27:535–540. [PubMed: 16819361]
4. Tsionos I, Leclercq C, Rochet JM. Heterotopic ossification of the elbow in patients with burns. Results after early excision. J. Bone Joint Surg. Br. 2004; 86:396–403.

5. Chakkalakal SA, Zhang D, Culbert AL, Convente MR, Caron RJ, Wright AC, Maidment AD, Kaplan FS, Shore EM. An *Acvr1* R206H knock-in mouse has fibrodysplasia ossificans progressiva. J. Bone Miner. Res. 2012; 27:1746–1756. [PubMed: 22508565]
6. Shore EM, Xu M, Feldman GJ, Fenstermacher DA, Cho TJ, Choi IH, Connor JM, Delai P, Glaser DL, LeMerrer M, Morhart R, Rogers JG, Smith R, Triffitt JT, Urtizberea JA, Zasloff M, Brown MA, Kaplan FS. A recurrent mutation in the BMP type I receptor ACVR1 causes inherited and sporadic fibrodysplasia ossificans progressiva. Nat. Genet. 2006; 38:525–527. [PubMed: 16642017]
7. Yu PB, Deng DY, Lai CS, Hong CC, Cuny GD, Bouxsein ML, Hong DW, McManus PM, Katagiri T, Sachidanandan C, Kamiya N, Fukuda T, Mishina Y, Peterson RT, Bloch KD. BMP type I receptor inhibition reduces heterotopic ossification. Nat. Med. 2008; 14:1363–1369. [PubMed: 19029982]
8. Culbert AL, Chakkalakal SA, Theosmy EG, Brennan TA, Kaplan FS, Shore EM. Alk2 regulates early chondrogenic fate in fibrodysplasia ossificans progressiva heterotopic endochondral ossification. Stem Cells. 2014; 32:1289–1300. [PubMed: 24449086]
9. Kronenberg HM. Developmental regulation of the growth plate. Nature. 2003; 423:332–336. [PubMed: 12748651]
10. Peterson JR, De La Rosa S, Sun H, Eboda O, Cilwa KE, Donneys A, Morris M, Buchman SR, Cederna PS, Krebsbach PH, Wang SC, Levi B. Burn injury enhances bone formation in heterotopic ossification model. Ann. Surg. 2014; 259:993–998. [PubMed: 23673767]
11. Zhang S, Kaplan FS, Shore EM. Different roles of GNAS and cAMP signaling during early and late stages of osteogenic differentiation. Horm. Metab. Res. 2012; 44:724–731. [PubMed: 22903279]
12. Sanvitale CE, Kerr G, Chaikuad A, Ramel MC, Mohedas AH, Reichert S, Wang Y, Triffitt JT, Cuny GD, Yu PB, Hill CS, Bullock AN. A new class of small molecule inhibitor of BMP signaling. PLOS One. 2013; 8:e62721. [PubMed: 23646137]
13. Bowler WB, Buckley KA, Gartland A, Hipskind RA, Bilbe G, Gallagher JA. Extracellular nucleotide signaling: A mechanism for integrating local and systemic responses in the activation of bone remodeling. Bone. 2001; 28:507–512. [PubMed: 11344050]
14. Miyazaki T, Iwasawa M, Nakashima T, Mori S, Shigemoto K, Nakamura H, Katagiri H, Takayanagi H, Tanaka S. Intracellular and extracellular ATP coordinately regulate the inverse correlation between osteoclast survival and bone resorption. J. Biol. Chem. 2012; 287:37808–37823. [PubMed: 22988253]
15. Moriatis JM, Gannon FH, Shore EM, Bilker W, Zasloff MA, Kaplan FS. Limb swelling in patients who have fibrodysplasia ossificans progressiva. Clin. Orthop. Relat. Res. 1997; 336:247–253. [PubMed: 9060511]
16. Liu Y, Berendsen AD, Jia S, Lotinun S, Baron R, Ferrara N, Olsen BR. Intracellular VEGF regulates the balance between osteoblast and adipocyte differentiation. J. Clin. Invest. 2012; 122:3101–3113. [PubMed: 22886301]
17. Peterson JR, Okagbare PI, De La Rosa S, Cilwa KE, Perosky JE, Eboda ON, Donneys A, Su GL, Buchman SR, Cederna PS, Wang SC, Kozloff KM, Morris MD, Levi B. Early detection of burn induced heterotopic ossification using transcutaneous Raman spectroscopy. Bone. 2013; 54:28–34. [PubMed: 23314070]
18. Davis AK, Kuhls DA, Wulff R, Fildes JJ, MacIntyre AD, Coates JE, Zamboni WA. Heterotopic ossification after blunt abdominal trauma. J. Trauma. 2008; 65:1536–1539. [PubMed: 18277276]
19. Sullivan MP, Torres SJ, Mehta S, Ahn J. Heterotopic ossification after central nervous system trauma: A current review. Bone Joint Res. 2013; 2:51–57. [PubMed: 23610702]
20. Salisbury E, Rodenberg E, Sonnet C, Hipp J, Gannon FH, Vadakkan TJ, Dickinson ME, Olmsted-Davis EA, Davis AR. Sensory nerve induced inflammation contributes to heterotopic ossification. J. Cell. Biochem. 2011; 112:2748–2758. [PubMed: 21678472]
21. Tannous O, Griffith C, O'Toole RV, Pellegrini VD Jr. Heterotopic ossification after extremity blast amputation in a Sprague-Dawley rat animal model. J. Orthop. Trauma. 2011; 25:506–510. [PubMed: 21738069]

22. Tannous O, Stall AC, Griffith C, Donaldson CT, Castellani RJ Jr. Pellegrini VD Jr. Heterotopic bone formation about the hip undergoes endochondral ossification: A rabbit model. Clin. Orthop. Relat. Res. 2013; 471:1584–1592. [PubMed: 23361932]

23. Hess K, Ushmorov A, Fiedler J, Brenner RE, Wirth T. TNFα promotes osteogenic differentiation of human mesenchymal stem cells by triggering the NF-κB signaling pathway. Bone. 2009; 45:367–376. [PubMed: 19414075]

24. Wang Q, Green RP, Zhao G, Ornitz DM. Differential regulation of endochondral bone growth and joint development by FGFR1 and FGFR3 tyrosine kinase domains. Development. 2001; 128:3867–3876. [PubMed: 11585811]

25. Gimble JM, Youkhana K, Hua X, Bass H, Medina K, Sullivan M, Greenberger J, Wang CS. Adipogenesis in a myeloid supporting bone marrow stromal cell line. J. Cell. Biochem. 1992; 50:73–82. [PubMed: 1339460]

26. Ninomiya Y, Sugahara-Yamashita Y, Nakachi Y, Tokuzawa Y, Okazaki Y, Nishiyama M. Development of a rapid culture method to induce adipocyte differentiation of human bone marrow-derived mesenchymal stem cells. Biochem. Biophys. Res. Commun. 2010; 394:303–308. [PubMed: 20206132]

27. Karunakar MA, Sen A, Bosse MJ, Sims SH, Goulet JA, Kellam JF. Indometacin as prophylaxis for heterotopic ossification after the operative treatment of fractures of the acetabulum. J. Bone Joint Surg. Br. 2006; 88:1613–1617. [PubMed: 17159174]

28. Bayliss J, Delarosa S, Wu J, Peterson JR, Eboda ON, Su GL, Hemmila M, Krebsbach PH, Cederna PS, Wang SC, Xi C, Levi B. Adenosine triphosphate hydrolysis reduces neutrophil infiltration and necrosis in partial-thickness scald burns in mice. J. Burn Care Res. 2014; 35:54–61. [PubMed: 23877144]

29. Cobb JP, Mindrinos MN, Miller-Graziano C, Calvano SE, Baker HV, Xiao W, Laudanski K, Brownstein BH, Elson CM, Hayden DL, Herndon DN, Lowry SF, Maier RV, Schoenfeld DA, Moldawer LL, Davis RW, Tompkins RG, Baker HV, Bankey P, Billiar T, Brownstein BH, Calvano SE, Camp D, Chaudry I, Cobb JP, Davis RW, Elson CM, Freeman B, Gamelli R, Gibran N, Harbrecht B, Hayden DL, Heagy W, Heimbach D, Herndon DN, Horton J, Hunt J, Laudanski K, Lederer J, Lowry SF, Maier RV, Mannick J, McKinley B, Miller-Graziano C, Mindrinos MN, Minei J, Moldawer LL, Moore E, Moore F, Munford R, Nathens A, O'keefe G, Purdue G, Rahme L, Remick D, Sailors M, Schoenfeld DA, Shapiro M, Silver G, Smith R, Stephanopoulos G, Stormo G, Tompkins RG, Toner M, Warren S, West M, Wolfe S, Xiao W, Young V. Inflammation and Host Response to Injury Large-Scale Collaborative Research Program, Application of genome-wide expression analysis to human health and disease. Proc. Natl. Acad. Sci. U.S.A. 2005; 102:4801–4806. [PubMed: 15781863]

30. Levi B, Nelson ER, Brown K, James AW, Xu D, Dunlevie R, Wu JC, Lee M, Wu B, Commons GW, Vistnes D, Longaker MT. Differences in osteogenic differentiation of adipose-derived stromal cells from murine, canine, and human sources in vitro and in vivo. Plast. Reconstr. Surg. 2011; 128:373–386. [PubMed: 21788829]

31. James AW, Xu Y, Wang R, Longaker MT. Proliferation, osteogenic differentiation, and FGF-2 modulation of posterofrontal/sagittal suture–derived mesenchymal cells in vitro. Plast. Reconstr. Surg. 2008; 122:53–63. [PubMed: 18594386]

32. Levi B, Hyun JS, Nelson ER, Li S, Montoro DT, Wan DC, Jia FJ, Glotzbach JC, James AW, Lee M, Huang M, Quarto N, Gurtner GC, Wu JC, Longaker MT. Nonintegrating knockdown and customized scaffold design enhances human adipose-derived stem cells in skeletal repair. Stem Cells. 2011; 29:2018–2029. [PubMed: 21997852]

33. Levi B, Nelson ER, Li S, James AW, Hyun JS, Montoro DT, Lee M, Glotzbach JP, Commons GW, Longaker MT. Dura mater stimulates human adipose-derived stromal cells to undergo bone formation in mouse calvarial defects. Stem Cells. 2011; 29:1241–1255. [PubMed: 21656608]

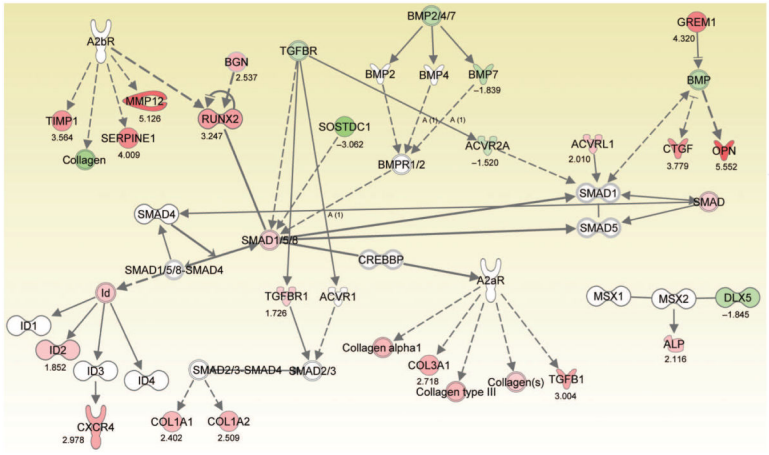

Fig. 1. Burn injury alters gene expression in adipose tissue

Schematic shows regulation and expression relationships between genes related to canonical SMAD signaling after burn injury. Within adipose tissue, 28 of 75 genes within the BMP-mediated SMAD canonical signaling pathway were up-regulated after burn injury (n = 244 burn patients, n = 35 control patients). Genes that were up-regulated at least twofold compared to controls are noted by red, whereas down-regulation of at least twofold compared to controls is indicated by green, with the actual ratio of up- or down-regulation indicated by the numbers below the gene names.

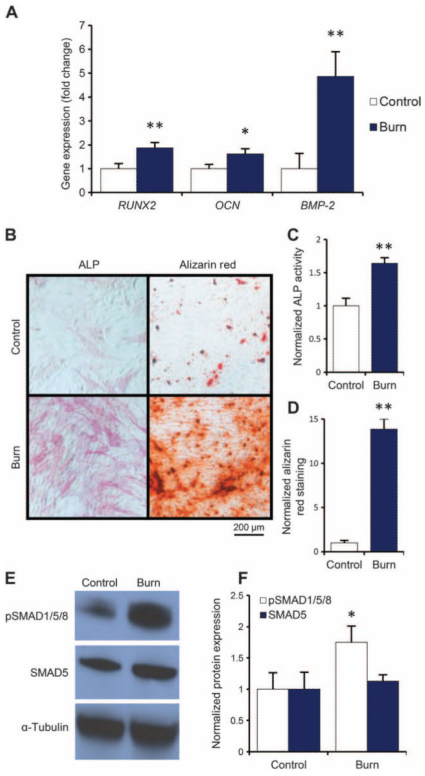

Fig. 2. Burn injury promotes the osteogenic differentiation of hMSCs

(**A**) Gene expression in hMSCs was assessed with quantitative reverse transcription polymerase chain reaction (qRT-PCR) of mRNA collected from human adipose-derived MSCs. Cells were derived from burn patients within the first 3 days of their burn injury (n = 3) and from age- and sex-matched control patients (n = 3). mRNA was harvested from the cells after 7 days of exposure to ODM and assessed for relative expression of osteogenic genes *RUNX2*, *OCN*, and *BMP-2*. Data are means ± SD. *RUNX2*, P = 0.008; *OCN*, P = 0.017; *BMP-2*, P = 0.005 (t test). (**B**) Micrographs of ALP and alizarin red staining of hMSCs after 7 and 14 days of exposure to ODM, respectively. Scale bar, 200 mm. (**C**) Quantification of ALP enzyme activity in burn and control hMSCs after 7 days of exposure to ODM. ALP activity was measured colorimetrically and normalized to total protein content for each group. Data are means ± SD (n =3 per group). P = 0.002 (t test). (**D**) Quantification of osteoid with alizarin red stain. Deposits were solubilized with cetylpyridinium chloride and analyzed colorimetrically. Data are means ± SD (n =3 per group). P = 0.001 (t test). (**E** and **F**) Western blot image (E) and analysis (F) of protein content in hMSCs after 7 days of exposure to ODM. Images were analyzed by densitometry and normalized to loading controls (α-tubulin). The ratio of phosphorylated (activated) SMAD protein (pSMAD1/5/8) to non-activated SMAD5 protein was increased in hMSCs from burn patients. Data are means ± SD (n = 3 per group). pSMAD1/5/8, P = 0.024; SMAD5, P = 0.490 (t test). *P < 0.05, **P < 0.01.

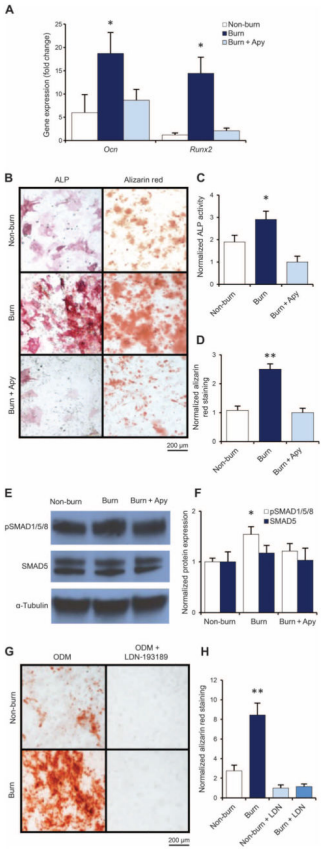

Fig. 3. Apyrase application at the burn site abrogates the osteogenic potential of mMSCs

(**A**) Gene expression in mMSCs was assessed by qRT-PCR of mRNA collected from mMSCs harvested 2 hours after burn injury, burn injury with immediate application of topical apyrase (Apy) solution, or exposure to room temperature water (non-burn control). mRNA was harvested from the cells after 7 days of exposure to ODM and assessed for the relative expression of osteogenic genes *Ocn* and *Runx2*. Data are means ± SD ($n = 3$ per group). *Ocn*, $P = 0.037$; *Runx2*, $P = 0.042$ [analysis of variance (ANOVA)]. (**B**) Micrographs of ALP and alizarin red staining of mMSCs after 7 and 14 days of exposure to ODM, respectively. Scale bar, 200 μm. (**C**) Quantification of ALP enzyme activity in burn, burn + apyrase, and non-burn control mMSCs after 7 days of exposure to ODM. ALP activity was measured colorimetrically and normalized to total protein content for each group. Data are means ± SD ($n = 3$ per group). $P = 0.018$ (ANOVA). (**D**) Quantification of osteoid deposition with alizarin red stain. Data are means ± SD ($n = 3$ per group). $P = 0.001$ (ANOVA). (**E** and **F**) Western blot image (E) and analysis (F) of protein content in mMSCs after 7 days of exposure to ODM. Images were analyzed by densitometry and normalized to loading controls (α-tubulin). Data are means ± SD ($n = 3$ per group). pSMAD1/5/8, $P = 0.047$; SMAD5, $P = 0.682$ (ANOVA). (**G** and **H**) Alizarin red stain (G) and quantification of osteoid deposition (H) of burn and non-burn mMSCs exposed to ODM for 2 weeks with or without supplementation with LDN-193189. Scale bar, 200 mm. Data are means ± SD ($n = 3$ per group). $P = 0.001$ (ANOVA). $^{*}P < 0.05$, $^{**}P < 0.01$.

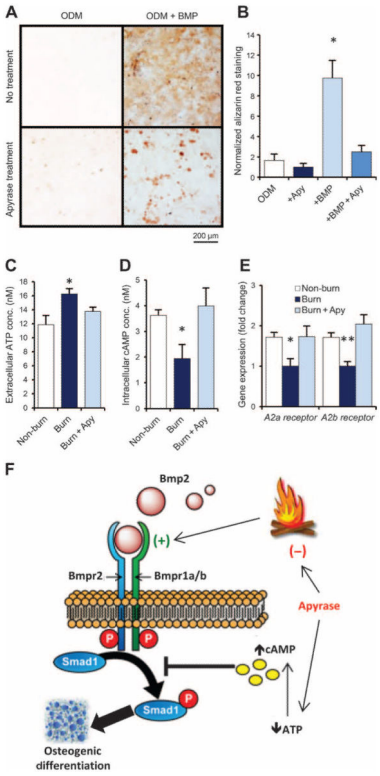

Fig. 4. Apyrase mitigates burn injury–induced osteogenic differentiation of MSCs by modulating ATP signaling

(**A** and **B**) Alizarin red stain (A) and quantification of osteoid deposition (B) of mMSCs collected from adipose tissue of untreated C57BL/6 mice and exposed to ODM with or without supplementation with recombinant BMP-2 ligand (200 ng/ml) and/or apyrase (4 U/ml). Scale bar, 200 μm. Data are means ± SD (n = 3 per group). P = 0.030 (ANOVA). (**C**) ATP assay for extracellular ATP concentrations in mMSC cultures harvested from the adipose tissue of mice 2 hours after burn injury, burn injury + topical apyrase treatment, or non-burn control (exposure to room temperature water). Data are means ± SD (n = 3 per group). P = 0.038 (ANOVA). (**D**) cAMP assay for intracellular cAMP from the same cells, showing that intracellular cAMP is reduced in MSCs from burn mice and up-regulated with apyrase treatment. Data are means ± SD (n = 3 per group). P = 0.018 (ANOVA). (**E**) Gene expression for the adenosine receptors *A2a* and *A2b* in the same mMSCs, assessed by qRT-PCR of mRNA collected after 7 days of exposure to ODM. Both adenosine receptors were down-regulated after burn injury, but this effect was absent in mice that received apyrase treatment or no burn. Data are means ± SD (n = 3 per group). *A2a* receptor, P = 0.011; A2b receptor, P = 0.004 (ANOVA). (**F**) Schematic showing BMP and ATP signaling interactions in HO formation after burn injury. Apyrase application after burn injury limits ATP and BMP signaling, thereby reducing the otherwise up-regulated osteogenicity of MSCs. *P < 0.05, **P < 0.01.

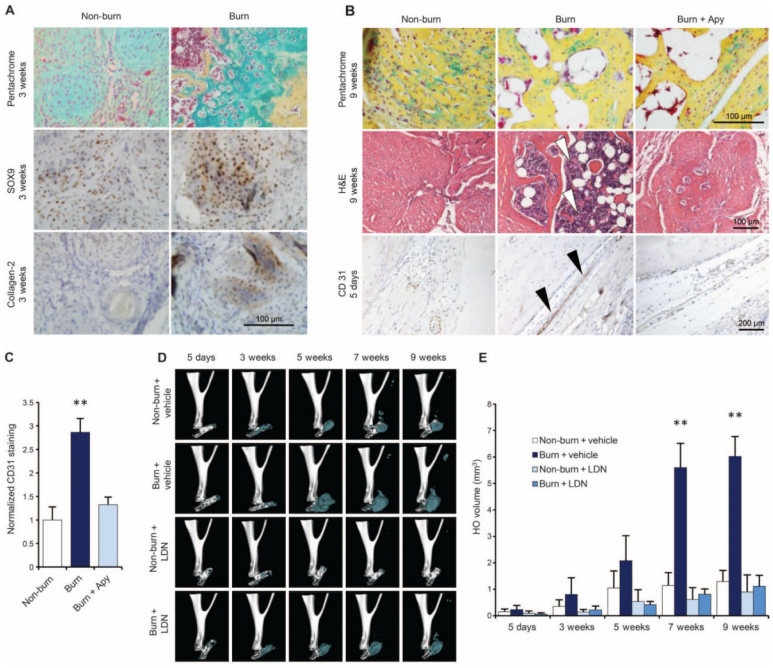

Fig. 5. Trauma-induced HO develops through an endochondral pathway and requires BMP signaling

(**A**) Photomicrographs of transverse sections of the tenotomy site 3 weeks after injury in mice with or without concurrent burn. Pentachrome (top) stains cartilage tissue in blue. Immunohisto-chemistry for SOX9 (middle) and collagen-2 (bottom) demonstrates positively staining cells in brown. Scale bar, 100 μm. (**B**) Pentachrome stain (top) of transverse sections through HO at the tenotomy site 9 weeks after injury from burn, burn + apyrase treatment, and non-burn control demonstrates mature bone (bright yellow), with cortical bone morphology most evident in burn mice. Cartilage appears blue. Scale bar, 100 μm. Hematoxylin and eosin (H&E) stain of transverse sections through HO (middle) at 9 weeks after injury demonstrates the development of mature bone marrow cavity (white arrowheads), suggesting its development from a multipotent precursor lineage. Scale bar, 100 μm. Vasculogenic signaling was assessed with CD31 (PECAM) immunohistochemistry on tangential sections through the tenotomy site before HO formation at 5 days after injury (bottom). Positively staining cells are brown (black arrowheads). Increased CD31 staining corresponded with the location of increased future HO development. Scale bar, 200 μm. (**C**) CD31 staining was quantified with Adobe Photoshop on five sequential tangential sections through the tenotomy site 5 days after injury. Data are mean $CD31^{+}$-stained pixels normalized between groups to show fold change ± SD (n = 3 per group). P = 0.001 (ANOVA). (**D**) Representative, reconstructed micro–computed tomography (μCT) scan images of the tenotomized legs of burn and non-burn mice, which received LDN-193189 (6 mg/kg, daily intraperitoneal injections) or vehicle control. Serial scans were completed at 5 days and 3, 5, 7, and 9 weeks after injury. Reconstructed images show new, ectopic bone formation in blue. (E) Quantification of non-native heterotopic bone in the lower extremity was performed at each scan time point. Data are means ± SD (n = 6 per group). P = 0.001 at 7 and 9 weeks (ANOVA). *P < 0.05, **P < 0.01.

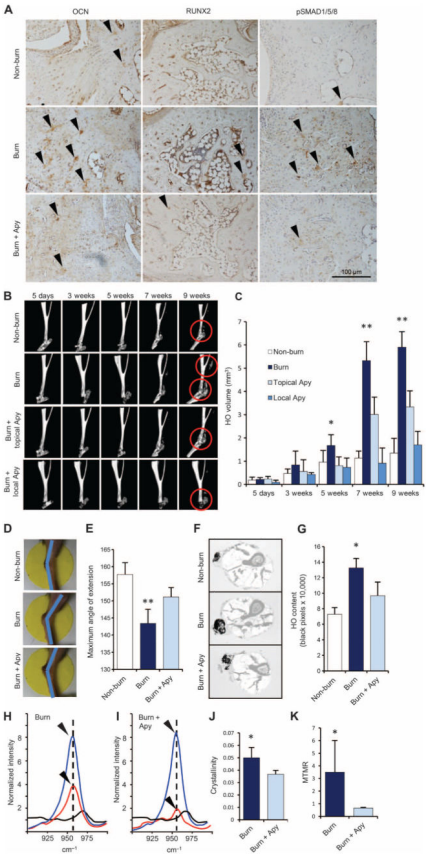

Fig. 6. Apyrase treatment decreases SMAD signaling and burn-induced ectopic bone mineral deposition

(**A**) Immunohistochemical staining in tissue sections harvested 5 days after injury from the region where μCT showed the most robust HO development at later time points. Arrows indicate positively staining cells for OCN (left), RUNX2 (middle), and pSMAD1/5/8 (right). Scale bar, 100 μm. (**B**) Representative, reconstructed μCT scan images of the tenotomized legs of burn, burn + apyrase (topical), burn + apyrase (local application at tenotomy), and non-burn mice shown at 5 days and 3, 5, 7, and 9 weeks after injury. Gray areas indicate regions of new, ectopic bone development; red circle indicates nidus of HO development. (**C**) Quantification of non-native heterotopic bone in the lower extremity was performed at each scan time point. Data are means ± SD (n = 6 per group, except for local apyrase group, for which n = 3). P = 0.037 at 5 weeks, P = 0.001 at 7 and9 weeks (ANOVA). (**D** and **E**) Images (D) and quantification (E) of the ROM, defined as maximum angle of extension, for the tenotomized leg 9 weeks after injury. Data are means ± SD (n =6 per group). P = 0.004 (ANOVA). (**F** and **G**) Representative transverse micrographs stained with aniline blue (F) of the tenotomy site 9 weeks after injury. Images were recolored to show gray pixels representing native bone and black pixels designating HO, which was quantified (G) at every 75 sections along the longitudinal axis of the tenotomized limb. Data are means ± SD (n =3 per group). P = 0.038 (ANOVA). (**H** and **I**) Ex vivo Raman spectroscopic analysis of cross-sections of the tenotomy site 9 weeks after injury. Blue curve indicates cortical bone, red curve indicates areas of predicted HO formation based on μCT scan images, and black curve indicates areas of soft tissue from mice receiving Achilles tenotomy + burn injury (H)

or tenotomy + burn with apyrase treatment at the burn site (I). Black arrows indicate intensity of the signal at the 958 cm^{-1} phosphate band. (**J** and **K**) Crystallinity (J) and mineral to matrix ratios (MTMR) (K) were significantly higher in the region of HO formation in untreated burn mice compared to burn mice receiving apyrase treatment. Data are means ± SD (n = 6 measurements, each measurement consisting of 10 spectra averaged over a 100-μm area of interest on cross-sections). Crystallinity, P = 0.015; MTMR, P = 0.021 (t test). *P < 0.05, **P < 0.01.